

Article

Mechanical Behavior and Permeability Evolution of Coal under Different Mining-Induced Stress Conditions and Gas Pressures

Zetian Zhang ^{1,2}, Ru Zhang ^{2,*} , Zhiguo Cao ^{1,3}, Mingzhong Gao ², Yong Zhang ¹ and Jing Xie ²

¹ State Key Laboratory of Water Resource Protection and Utilization in Coal Mining, China Energy Investment Co. LTD, Beijing 100011, China; znthe123@126.com (Z.Z.); zgcao2008@163.com (Z.C.); sklwu_zy2020@126.com (Y.Z.)

² MOE Key Laboratory of Deep Earth Science and Engineering, College of Water Resource and Hydropower, Sichuan University, Chengdu 610065, China; gmzh@scu.edu.cn (M.G.); xiejing200655@163.com (J.X.)

³ National Institute of Clean-and-Low-Carbon Energy, Beijing 102211, China

* Correspondence: zhangru@scu.edu.cn; Tel.: +86-28-8546-3228

Received: 22 April 2020; Accepted: 18 May 2020; Published: 26 May 2020



Abstract: The gas permeability and mechanical properties of coal, which are seriously influenced by mining-induced stress evolution and gas pressure conditions, are key issues in coal mining and enhanced coalbed methane recovery. To obtain a comprehensive understanding of the effects of mining-induced stress conditions and gas pressures on the mechanical behavior and permeability evolution of coal, a series of mining-induced stress unloading experiments at different gas pressures were conducted. The test results are compared with the results of conventional triaxial compression tests also conducted at different gas pressures, and the different mechanisms between these two methods were theoretically analyzed. The test results show that under the same mining-induced stress conditions, the strength of the coal mass decreases with increasing gas pressure, while the absolute deformation of the coal mass increases. Under real mining-induced stress conditions, the volumetric strain of the coal mass remains negative, which means that the volume of the coal mass continues to increase. The volumetric strain corresponding to the peak stress of the coal mass increases with gas pressure in the same mining layout simulation. However, in conventional triaxial compression tests, the coal mass volume continues to decrease and in a compressional state, and there is no obvious deformation stage that occurs during the mining-induced stress unloading tests. The theoretical and experimental analyses show that mining-induced stress unloading and gas pressure changes greatly impact the deformation, failure mechanism and permeability enhancement of coal.

Keywords: coalbed methane; mining-induced stress unloading; gas pressure; mechanical behavior; permeability evolution

1. Introduction

According to the specific report from the Intergovernmental Panel on Climate Change, human activities are estimated to have caused approximately 1.0 °C of global warming above pre-industrial levels, and global warming is likely to reach 1.5 °C between 2030 and 2052 if it continues to increase at the current rate [1,2]. The emission of carbon dioxide (CO₂) is considered to be the main cause of the greenhouse effect and global warming [3]. However, researches also show that the coalbed methane (CBM) is not just a major source of energy [4] but also one of the most harmful greenhouse gases [5,6], whose the greenhouse effect is 21–34 times that of carbon dioxide (CO₂) [7,8]. To prevent the mining-induced CBM excessive emission from causing environmental problems and greenhouse effects, the CBM should be pre-extracted and utilized, and a CO₂-enhanced coalbed methane (CO₂-ECBM)

extraction technology is founded and used in the coal mining and CO₂ storage practice [9,10] faced with a great demand of decreasing CO₂ emissions.

However, with the rapid development of China, the shallow coal resources is continually exhausting, resulting in a rapid increase in mining depth. During deep coal mining, the in situ stress and CBM pressure significantly increase, and the coal mass presents obvious nonlinear mechanical behavior resulting in a difficulty in conducting the CO₂-ECBM. Nevertheless, most existing theories are founded by conducting conventional triaxial compression (CTC) tests, and complete stress-strain relationships are used to analyze and describe the basic mechanical behavior and failure damage process [11–14]. That is a static research mean used to obtain the basic mechanical parameters and properties of the rock material. The advantage of the method is that the test results are comparable. The disadvantage of the method is the ignorance of the great influence of the in situ stress state and mining-induced disturbance, the engineering activities are considered separately, and the real mechanical response of the rock mass under engineering disturbance or operation conditions is not quantitatively considered [15,16]. The essential reason for the deformation, failure and instability of a deep rock mass is that underground mining or excavation activities break the occurrence stress balance in the rock mass, and the mechanical behavior of a deep rock mass is closely related to mining layout, excavation or mining-induced disturbance [16].

Based on Xie's study [15], assuming that the deep coal seam originates in a hydrostatic pressure state, the pressure distribution ahead of the mining face can be described for simplification as follows: with the decrease in distance from the mining face, the vertical stress acting on the coal seam gradually increases to a peak stress from the hydrostatic pressure state and then quickly decreases due to coal mass damage; the horizontal stress gradually decreases to 0 from the hydrostatic pressure state, ignoring the stress rotation and fluctuation near the mining face due to rock failure [17]. The seepage and mechanical property of the coal mass is seriously stress-dependent [18–20], indicating that in the seepage mechanics behavior of the coal mass is deeply influenced by the actual mining-induced stress evolution processes.

The implementations of different mining layouts led to differential distributions of the coal mining stress environment in front of the working face, which greatly affects coal fracture network formation and leads to large changes in the coal's permeability. The whole evolution process is the result of the coupling effect of seepage and stress, which directly affects the safety and reliability of simultaneous coal and gas extraction and the design and selection of mining processes [21]. However, the basic theory of existing coal mechanics is based on the study of the intrinsic mechanical behavior of coal at the material level based on traditional mechanical testing. This theory considers coal as only a kind of engineering material and cannot consider the effects of real and different mining layouts (disturbances), and most of the research results cannot describe the mechanical properties and seepage characteristics of coal under real mining conditions [22]. Therefore, the effect of the in situ stress state and mining-induced stress evolution must be considered in studies on the disturbance processes of engineering activity and the mechanical response of a deep rock mass.

The mechanical behavior and permeability evolution characteristics of coal under the impact of the mining-influenced stress environment are of major concern in the deep coal mining practice and CBM extractions. Scholars have comprehensively studied the problem by means of theoretical modeling, experimental simulation and numerical analysis. To investigate the influence of the effective stress coefficient and gas sorption-induced strain on coal permeability, Chen et al. [23] conducted an adsorption or desorption gas permeability experiment under constant confining pressure and pore pressure differences, and the coal permeability model of adopted stress variation conditions was founded, which differed from existing models based on uniaxial strain conditions, i.e., the Palmer-Mansoori model [24], Shi-Durucan model [25] and Cui-Bustin model [26]. Ju et al. [27] conducted an experimental study on CH₄ permeability and its dependence on the interior fracture networks of fractured coal under different excavation stress paths. A triaxial testing machine and microfocus computed tomography (μ CT) were used to measure the permeability of the fractured coal and to identify dynamic changes

in the interior fracture network under typical excavation loads. Islam et al. [28] presented numerical simulations to evaluate stress redistribution, water inflow enhancements and strata failure that result from underground coal mining in Barapukuria and showed that the multislice extraction of coal would introduce large amounts of caving in the mine roof. Zhang et al. [29] built a three-dimensional numerical extraction model based on the geologic and mining conditions of a specific coal mine and explored the mining-induced localized stress concentration and interlayer rock failure behavior using field investigations and numerical calculation methods. Wold et al. [30] conducted in situ well tests, statistical analyses and mechanistic-stochastic outburst modeling of gas flow and outburst during coal mining and explored the role of spatial variability in coal seam parameters on gas outburst behavior; their research indicated that the permeability and strength field variabilities can lead to both outburst and nonoutburst outcomes from the same measured input data due to different spatial distributions of permeability and strength at the face. Singh et al. [31] performed field monitoring at 16 depillaring faces with depths ranging from 44 to 244 m, and the geomechanical properties of the overlying roof strata of each site were also determined, which shows that monitoring mining-induced stress during depillaring under massive and strong roofs is of considerable importance for safety. Zhang et al. [32] conducted in door and in situ experimental researches on the mechanical behavior and permeability of coal under different degrees of unloading confining pressure and reloading axial stress, which shows obvious differences in mechanical response with the testing results obtained by CTC tests. According to these studies, coal mining practices can seriously influence the stress field of the coal seams, which also determines the stress-dependent coal properties but is not quantitatively considered in experimental and theoretical analyses.

Faced with the problem of the mining-induced stress evolution influence on the mechanical behavior of a coal mass, Xie et al. [15] revealed the properties of abutment pressure at a longwall coal face under the three typical mining layouts, i.e., top coal caving mining (TCM), non-pillar mining (NM) and protective coal seam mining (PCM); the researchers suggested a mining-induced stress state of the coal mass in front of the mining face to determine the loading and unloading parameters for a laboratory study involving different mining layouts. Following this study, some scholars conducted studies on the mechanism of deformation-induced damage, fracture geometry and gas permeability enhancement of coal under typical mining layouts using a combination of theoretical, numerical and experimental methods [33–35]. Zhang et al. [22,36] explored the coal permeability evolution under different mining layouts and founded an anisotropic coal permeability model that considers mining-induced stress evolution, microfracture propagation and gas sorption/desorption effects. Based on these studies, the mining-induced mechanical behavior and permeability evolution of a coal mass were analyzed, and some new understanding of the real mining-influenced coal properties has been presented. However, the effects of gas pressure on the real mining-induced coal permeability enhancement and mechanical behavior has not been fully considered in these studies.

The coal seams in China often have high gas content and pressure, especially the deep coal seams, e.g., the Furong coal mine in Sichuan Province. The effective utilization of coal-gas simultaneous extraction technology is facing with the limits of unsystematic cognition of real mechanical responses of coal under different mining-induced stress and gas pressure conditions. Facing the needs of mining practice, it is of great significance to conduct studies considering the influences of different mining-induced stress unloading (MSU) conditions and gas pressures. Based on exploration of the differential evolutions of stress and environmental conditions in coal mass induced by different mining layouts, a mechanical test of the mining-induced stress behavior of coal during different mining methods can be designed, and then, the real seepage mechanical behavior of a coal mass under different mining-induced stress conditions can be obtained, providing theoretical and technical guidance for the implementation of coordinated coal and gas simultaneous extraction.

2. Materials and Methods

2.1. Sample Preparation

To obtain the mechanical characteristics of mining-induced coal mass stress and maintain more representative research results, the coal samples were collected from two different mining areas, i.e., the Furong coal mine in the Sichuan Province and the Tashan coal mine in the Shanxi Province, according to the descriptions of the American Society for Testing and Materials standard [37]. The sampling depths range from 300 m to 500 m, and the main coal mass components are shown in Tables 1 and 2. All the coal samples were drilled in the direction parallel to the bedding planes and numbered with the mining-induced stress condition (first chapter), i.e., NM, TCM and PCM and the gas pressure (the first number) and testing order (the second number). For example, the coal sample P-2-2 is the second coal sample used to conduct the experimental simulation of the PCM stress evolution process under a gas pressure equal to 2 MPa.

Table 1. Properties of the Baijiao anthracite samples [22].

Proximate Analysis					
Fixed carbon	Volatile matter		Ash		
75.17%	7.64%		16.38%		
Ultimate Analysis					
Carbon	Hydrogen	Nitrogen	Sulfur	Oxygen	
89.56%	2.7%	1.13%	2.97%	3.64%	
Constituent of Mineral Matter					
Kaolinite	Quartz	Calcite	Others		
5.58%	11.74%	5.04%	77.64%		
Sample Physical Properties					
Sample No.	Diameter (mm)	Length (mm)	Density (g/cm ³)	Gas pressure (MPa)	
N-0-1	50.13	98.78	1.51	0	
N-2-1	50.14	97.23	1.44	2	
T-0-1	50.00	97.91	1.49	0	
T-2-1	50.09	99.42	1.50	2	
T-2-2	50.16	98.23	1.48	2	
P-0-1	50.08	97.63	1.56	0	
P-0-3	49.64	100.77	1.50	0	
P-2-1	50.17	99.97	1.45	2	
P-2-2	50.07	100.09	1.48	2	
P-2-3	50.09	99.86	1.46	2	

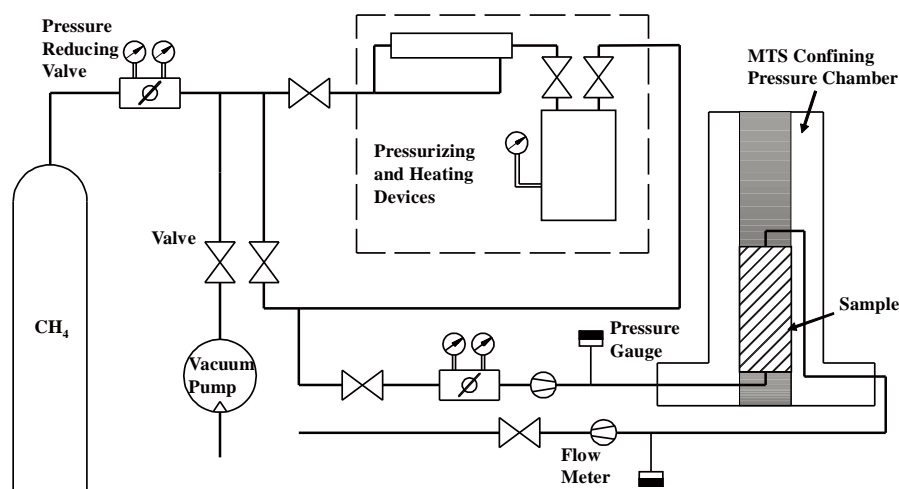
2.2. Testing Methods and Facility

2.2.1. The Testing Facility

The MTS-815 rock mechanics testing system (Sichuan University, Chengdu, China) equipped with a self-designed external gas flow system (Figure 1) was employed to conduct the stress unloading experiments [38]. This apparatus has a high maximum axial compression load (up to 4600 kN), high stiffness (10.5×10^9 N/m), high load-sensing accuracy (10 N) and high deformation-sensing accuracy (1 μ m). The testing ranges of the confining stress and axial and circumferential deformation extensometers are 0–140 MPa, –2.5 to +5.0 mm and –2.5 to +8.0 mm, respectively. The testing range for the pore pressure and the methane flow rate are 0.3–20 MPa and 5–5000 mL/min, respectively, with a sensing accuracy of 1% full scale.

Table 2. Properties of the Tashan bituminous coal samples.

Proximate Analysis				
Fixed Carbon	Volatile matter		Ash	
49.74%	33.23%		15.93%	
Ultimate Analysis				
Carbon	Oxygen	Silicon	Aluminium	Calcium
58.7%	27.5%	4.44%	4.27%	2.79%
Constituent of Mineral Matter				
Kaolinite	Siderite	Calcite	Others	
71%	3.77%	22.54%	2.69%	
Sample Physical Properties				
Sample No.	Diameter (mm)	Length (mm)	Density (g/cm ³)	Gas pressure (MPa)
N-2-2	47.74	102.46	1.31	2
T-2-3	47.65	97.99	1.44	2
P-2-4	47.65	102.48	1.44	2
N-1-1	47.69	98.23	1.54	1
T-1-1	47.67	101.35	1.61	1
P-1-1	47.69	102.17	1.49	1
N-0-2	47.70	100.64	1.52	0
T-0-2	47.65	100.35	1.57	0
P-0-4	47.64	100.65	1.57	0

**Figure 1.** Schematic sketch of the self-designed external gas flow system used in the tests [38].

2.2.2. Laboratory Simulations of Different Mining-Induced Stress Conditions

To simulate the real mining-induced stress and gas flow conditions under different mining layouts, we have used similar testing methods to those of Xie et al. [15], in which the mining-induced stress evolutions under three different mining layouts have been quantitatively analyzed and simulated. However, the continuous evolution processes of gas pressure in coal seams are complex and hard to be quantitatively described. Therefore, the gas pressures are set to 0, 1 and 2 MPa to provide a good understanding of the gas pressure effects on the real mining-induced seepage mechanical behavior of the coal mass. The detailed experimental settings are the same as those in Xie's work [15], and the difference is that the gas pressure has been set as a variable and the premining unloading process of the coal mass under PCM is also simulated in the experiments to show the effects of mining the

protective coal seam. The loading paths are shown in Figures 2 and 3, and all the coal specimens have experienced different mining-induced stress evolutions on a laboratory scale.

For comparison with the experimental results of the mining-induced coal samples, CTC tests were also conducted at different gas pressures, i.e., 0.5, 1.0 and 2.0 MPa. The confining pressure is set as 12 MPa, corresponding to a sampling depth of 500 m with a gradient of 25 kPa/m. The CTC test was conducted with a constant circumferential deformation rate of 0.08 mm/min until the residual strength was reached.

To uniformly control the initial gas adsorption/desorption state in the coal mass, the coal samples were initially loaded with an axial stress equal to 2 kN, and the confining pressure was loaded to 25 MPa with a constant rate of 3 MPa/min. During confining oil filling and pressure loading, the input and output pipes were evacuated after approximately 60 min. When the confining pressure stabilized, the gas pressure was loaded and kept constant for approximately 120 min to guarantee saturated gas adsorption of the coal samples.

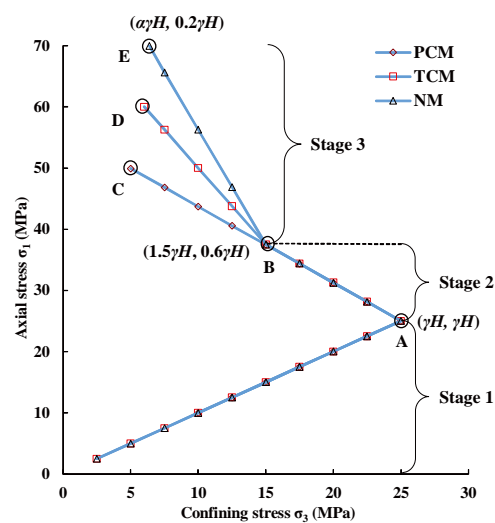


Figure 2. The stress unloading paths of different mining-induced stress conditions [39].

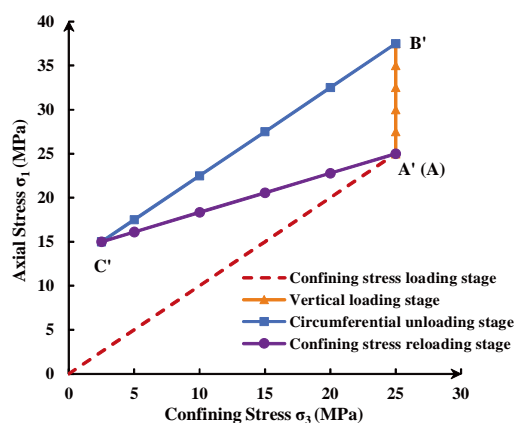


Figure 3. The simulation stress path of the premining unloading process in PCM [22].

2.3. Formulation of the Rock Permeability Evolution

According to the experimental setting, we can assume that gas permeation through the sample is an isothermal process, then the ideal gas law applies. The compressible gas permeability can be calculated from [40]:

$$k = \frac{2qp_0\mu_v L}{A(p_1^2 - p_2^2)} \quad (1)$$

where k is the coal permeability, m^2 ; q is the volumetric rate of flow at reference pressure, m^3/s ; p_0 is the reference pressure, which is set as the atmospheric pressure in this work, i.e., 0.101325 MPa; A is the cross section of the core plug sample, m^2 ; μ_v is the viscosity coefficient of gas and equals 1.087×10^{-5} Pa·s when the temperature is 20 °C; L is the length of the coal specimen, m; and p_1 and p_2 are the input and output gas pressures, respectively, MPa.

3. Results

3.1. The Mechanical Behavior and Gas Permeability in Coal under the Conventional Triaxial Stress Condition

3.1.1. The Mechanical Behavior of Coal under Different Gas Pressures

The CTC testing results under gas flow conditions are shown in Table 3, which shows that six coal specimens were successfully tested, while only three of the specimens recorded the completed seepage process. The other three specimens had no measured effective gas permeation. The images before and after coal damage are shown in Figure 4.

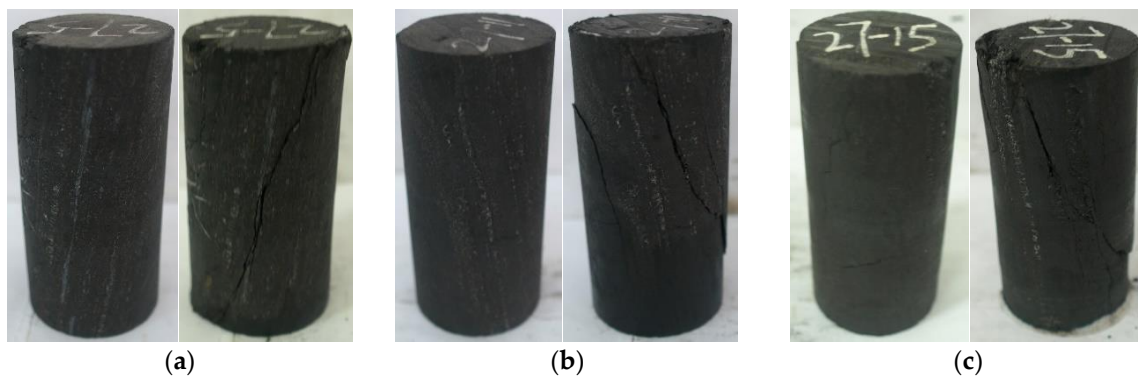


Figure 4. Comparison of coal samples before and after testing under different gas pressures: (a) 27-5 (0.5 MPa); (b) 27-11 (1 MPa); (c) 27-15 (2 MPa).

According to Figure 4, the initial coal fractures are parallel to the coal specimen axis. However, because of the fine filling between the fracture structure, the initial coal permeability is quite low. Comparing the images before and after coal sample failure, the coal mass is loaded and destroyed under the triaxial gas flow conditions and shows typical compression-shear failure characteristics. The shear failure surface intersects the initial fracture structure surface at a small angle. Based on Zhang et al.'s work [41], macroscopic damage usually begins with natural fracture structure defects or stress concentration areas. The initial natural fracture structure distribution also has a significant impact on the macroscopic failure location of the coal sample and the distribution of the fracture network under triaxial loading conditions. Whether the macroscopic fracture networks of the coal sample are distributed in the axial direction determines the test results of the macroscopic gas migration process in the coal sample and the coal's mechanical characteristics.

Table 3. Basic information and test results of coal samples under CTC conditions.

Sample Number	Average Diameter/mm	Average Length/mm	Density g/cm ³	Gas Pressure/MPa	Peak Strength/MPa	Strain Corresponding to Peak Strength/%			Residual Strength/MPa	Elastic Modulus/GPa	Poisson's Ratios	Permeability Corresponding to Peak Strength/mD	Perk Permeability/mD
						ϵ_1	ϵ_3	ϵ_v					
27-16	47.63	101.05	1.47	0.5	61.54	1.18	−0.34	0.51	53.00	72.95	0.395	0.0670	1.8034
27-5	47.62	99.08	1.52	0.5	67.99	1.14	−0.55	0.03	51.74	66.13	0.404	No effective penetration during loading	
27-14	47.65	100.53	1.50	1.0	63.84	0.96	−0.43	0.09	48.58	78.18	0.407	0.3639	2.4328
27-11	47.62	100.84	1.51	1.0	65.35	2.01	−0.81	0.40	49.50	67.70	0.411	No effective penetration during loading	
27-15	47.72	100.96	1.67	2.0	55.40	1.38	−0.45	0.48	47.00	101.62	0.395	0.1545	0.2227
19-5	47.75	101.55	1.33	2.0	70.91	1.34	−0.56	0.22	57.00	54.02	0.427	No effective penetration during loading	

3.1.2. The Gas Permeability Characteristics of Coal under Triaxial Compression Stress Conditions

The permeability evolutions of the coal samples under triaxial compression stress conditions with different gas pressures (0.5 MPa, 1 MPa and 2 MPa) are successfully recorded and shown in Figure 5. The testing results show a typical permeability evolution pattern similar to that of other relevant studies, i.e., the permeability of the coal mass under triaxial compression stress conditions first decreases with an increase in axial stress due to the compaction of pores and fractures in coal. Then, the coal permeability will recover and increase when the axial stress is larger than the yield stress and the corresponding volume expansion of the coal samples appears. The coal permeability will increase in post-peak stress loading section, while, the increasing rate of the coal permeability shows an obvious decrease comparing with the pre-peak loading section. Then the increasing rate of the coal permeability remains constant when the axial stress equals the residual strength.

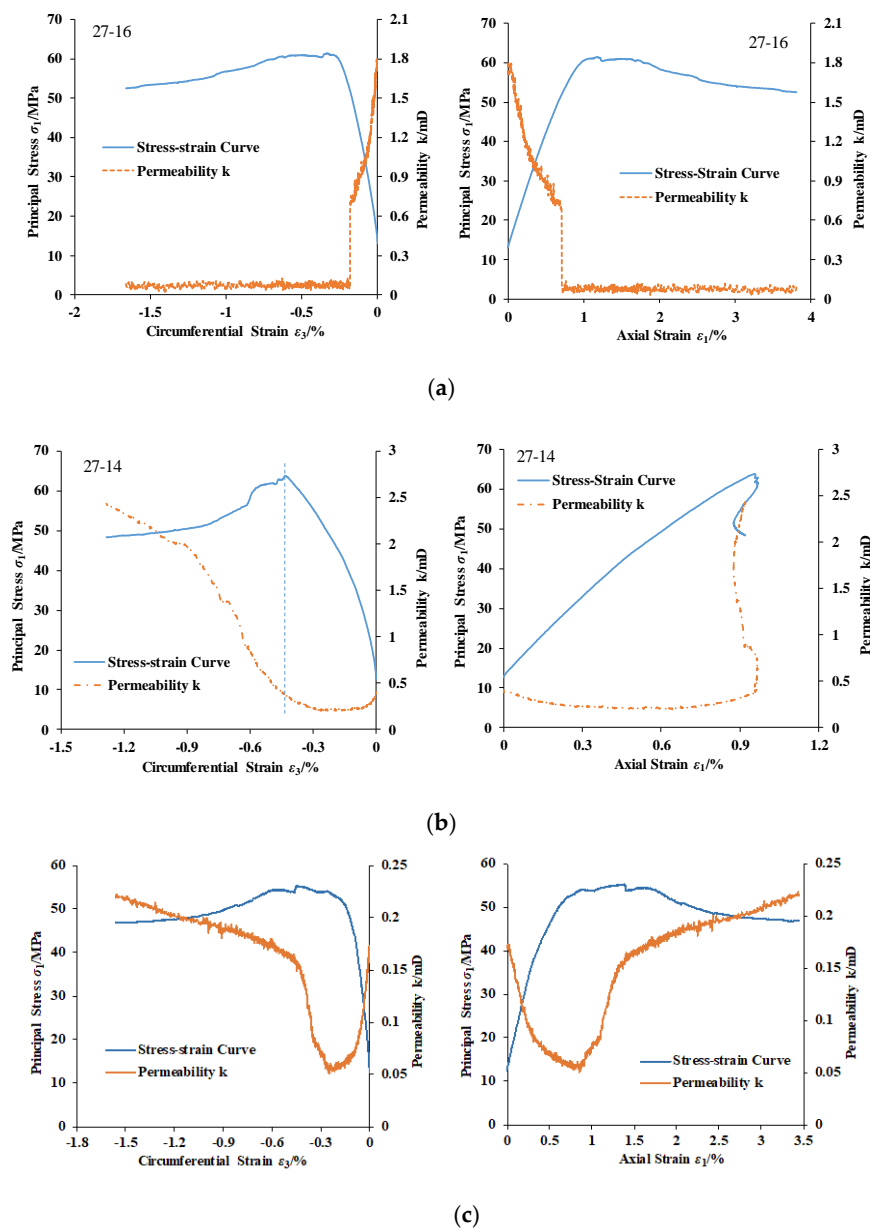


Figure 5. Relationship between permeability and axial strain or circumferential strain during loading of coal: (a) 27-16 (0.5 MPa); (b) 27-14 (1 MPa); (c) 27-15 (2 MPa).

The internal cracks of the coal specimens expand and penetrate into the peak stress section, which promotes the significant enhancement of coal permeability. However, with the advance in the loading process, the coal samples are further broken, some of the existing seepage channels are destroyed and the growth rate of the coal permeability slows. According to engineering practice, the coal mass near the working face underwent a complicated mining influence before mining, and the coal permeability has a certain elevation compared with that before mining.

According to Figure 5a, the permeability of coal sample 27-16 suddenly declined under loading and then no longer increased and remained near the lower limit of instrument measurement. This result shows that during the loading process, the seepage channel is suddenly destroyed with the process of loading and failure, and the gas cannot pass through the coal mass during the process of subsequent loading. Considering the test results of other coal samples, the permeability of the coal matrix is low, and the coal fractures are the main gas flow channels in the coal. Once the seepage channels are destroyed during the process of loading and failure, the coal permeability will significantly decrease, and then, the gas will be transferred to other locations and the corresponding gas pressure will increase, resulting in local gas accumulation and paroxysmal excess.

Additionally, the final coal permeability is typically larger than the initial permeability, which shows that the coal fracture network is expanded and the permeability is generally improved during the loading process. Therefore, the partial loading or unloading of coal can induce coal fracturing and permeability enhancement. The permeability evolution under different loading states also shows that the coal is highly stress-dependent and of high stress sensitivity. However, the conventional triaxial stress loading conditions are not the real mining-induced stress environment. To better understand the real mechanical and seepage characteristics of coal, mining-induced stress conditions should be seriously considered in these studies.

3.1.3. The Effects of Gas Pressure on the Mechanical Behavior of Coal under Triaxial Stress Conditions

According to the test results shown in Table 3, the triaxial compressional peak strength of coal samples drilled from the same coal blocks decreases with increasing gas pressure, resulting in an effective stress decrease. Under the same gas pressure conditions, the peak strength and residual strength of most nonpermeable coal samples are obviously higher than those of the permeable coal samples. The gas flow in the coal mass is mainly carried through the fracture network, and the connected fracture network usually affects the strength and deformation characteristics of coal, and coal with a developed fracture network usually has a lower strength, which fits well with the above testing results.

In addition, the residual strength of the coal samples with the measured gas flow process decreases with increasing gas pressure. Most of the coal failure under triaxial compression conditions is shear failure, the residual strength is determined by the shear strength of the failure surface, and the shear strength is positively correlated with the shear face stress. The greater the gas pressure, the smaller the effective positive stress on the shear surface of coal, and the smaller the shear strength of the failure surface.

Under different gas pressure conditions, the volume strains corresponding to the peak stress of coal samples are all positive, which means that the coal is in the volume compression state when the axial load reaches the peak stress. The complete stress-strain curves of triaxial coal samples are shown in Figure 6. The figure shows that the different gas pressures have little influence on the deformation properties of coal under the test setting conditions, and the deformation corresponding to the coal strength does not change with the change in gas pressure, which is related to the specificity of the coal specimen. The deformation properties of the coal samples are mainly controlled by the initial pore distribution and the final failure form. The initial fracture distribution of the coal sample has an obvious influence on the triaxial mechanical properties and seepage characteristics.

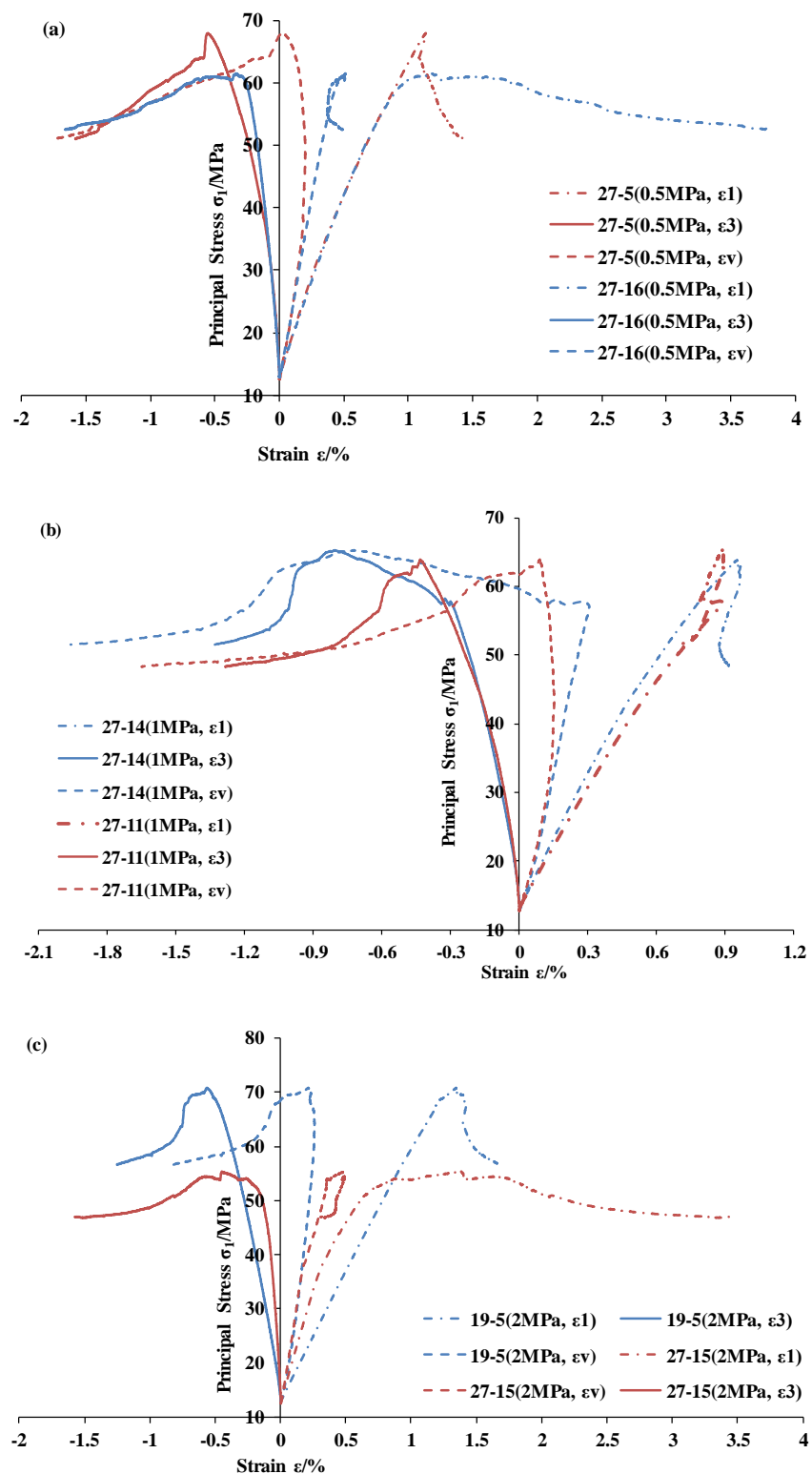


Figure 6. Complete stress-strain curves of CTC coal samples with different gas pressures: (a) 0.5 MPa; (b) 1 MPa; (c) 2 MPa.

The effects of gas pressure on the mechanical and seepage characteristics under triaxial stress conditions can be divided into two parts: the effects on the effective stress and peak strength and the effects on the gas adsorption and sorption-induced coal matrix deformation. According to Biot’s effective stress theory [42], the effective stress will decrease with increasing gas pressure, the average

peak strength and residual strength of the coal samples will correspondingly decrease, and the average Poisson's ratio increases, which fits well with the test results shown in Table 3 and indicates that the mining-induced peak stress and residual stress of coal mass near the mining face with high gas pressure are correspondingly low, while the deformation ability is enhanced. The coal mass in high gas pressure area is more prone to instability, deformation and failure. The test results also show that the initial amount and evolution range of coal permeability decrease with increasing gas pressure due to gas sorption-induced coal matrix swelling and coal fracture aperture decrease, which can introduce a geometric decline in coal permeability.

Although the gas pressure in the test is low, the difference in gas pressure still has an effect on the mechanical properties of coal. As an adsorptive primary gas, CBM has a great influence on the mechanical properties of fractured coal, which is always the most relevant factor in coal mining and CBM extraction. Therefore, when dealing with the fractured coal engineering problem, the influence of gas pressure and other related factors should be considered. The coal samples have significant individual differences, which determines the initial structure and mechanical property differences in the coal mass, resulting in a discrete distribution of the test results.

3.2. Mechanical Responses and Gas Permeability Properties of Coal under Different MSU Conditions

3.2.1. The Mechanical Behavior of Coal under Different MSU Conditions

Based on the abovementioned experimental simulation methods, a series of indoor experimental simulations of three typical MSU conditions have been conducted to obtain a compression understanding of the real mining-influenced mechanical behavior of coal masses under different gas pressures. The complete stress-strain curves of a typical coal sample (N-2-1) with a mining-induced stress condition simulation are shown in Figure 7, which is different from the CTC test results.

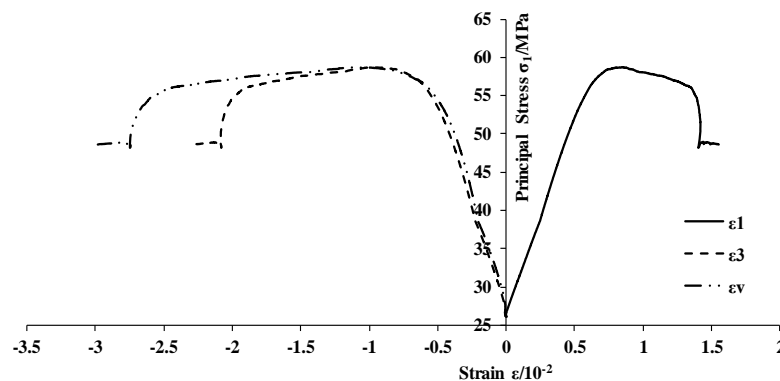


Figure 7. Mining-induced stress-strain curve of a coal sample (N-2-1).

Under the three typical MSU conditions, all the stress-strain curves show obvious deformation stages near the peak stress, and the volume deformation not only appears to be the volume compression in the initial compression stage but also the significant volume expansion at the loading and failure stages, which is different from the volume compression during the whole CTC loading process. In the CTC tests, the coal samples typically have obvious volume compression and brittle characteristics, while in the MSU tests, the plastic characteristics and volume expansion of mining-induced coal are better. The real mechanical behavior of mining-induced coal is not the mechanical property of the coal considering a typical material but the mechanical response under real mining-induced stress and gas flow conditions.

The peak stress deformation stage of the coal sample is more obvious when the gas pressure increases; that is, the greater the gas pressure, the more significant the deformation of the coal sample in the peak stress zone, according to the deformation curves (Figure 8) of the Tashan coal samples under conditions of different mining-induced stresses and gas pressure conditions.

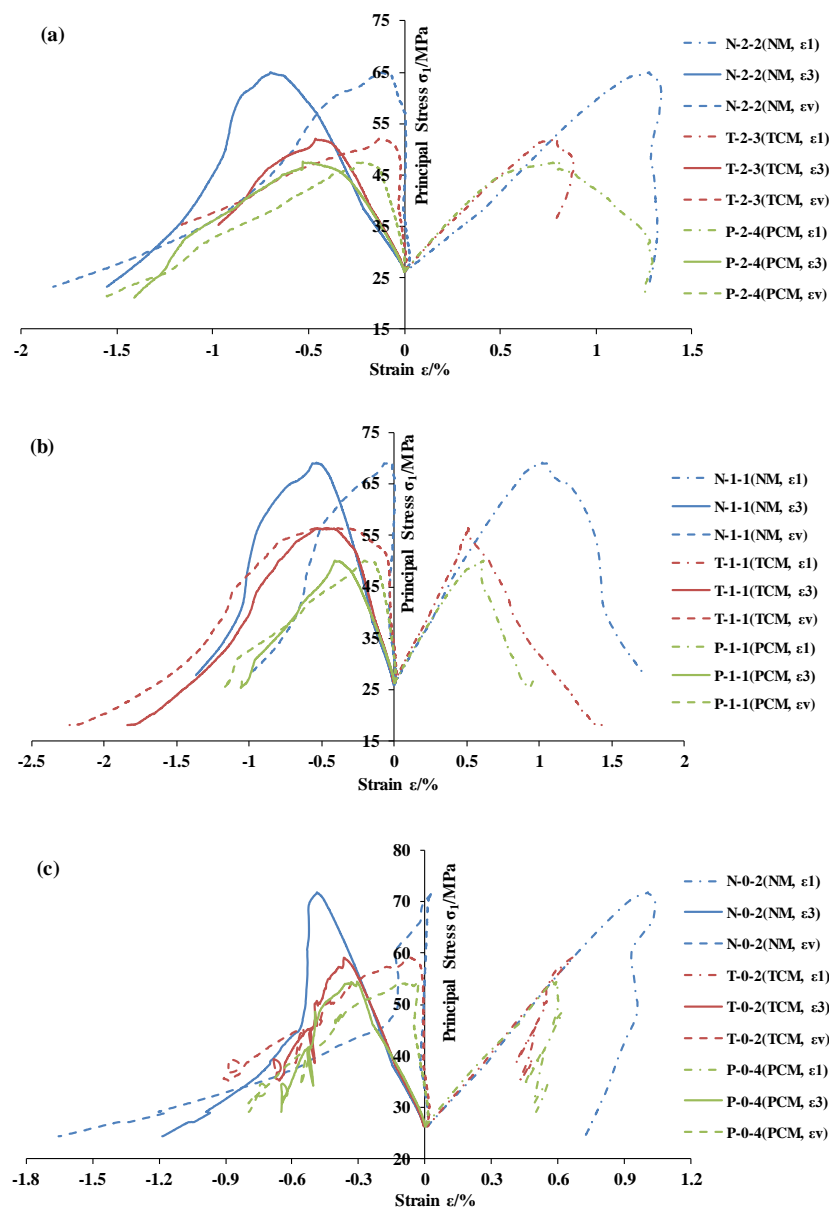


Figure 8. The mining-induced stress-strain curves of coal samples collected from the Tashan mining area under different mining-influenced conditions: (a) 0 MPa; (b) 1 MPa; (c) 2 MPa.

With the effects of gas, the deformability of the coal sample is improved. On the one hand, this improvement is due to the adsorption of coal to gas. The coal sample expands, and the deformation capacity increases after the coal samples adsorb gas; on the other hand, the greater the gas pressure, the smaller the effective confining pressure of the coal samples, and the larger the deformation of the coal samples in the same stress state. From another viewpoint, the smaller the gas pressure, the easier it is for the coal to suddenly lose its stability in the peak stress area. The occurrence of gas in the coal seam enables good deformability in the coal. However, mining practices will disrupt the initial equilibrium state, and the gas escapes and moves because mining or extraction will result in the corresponding effective stress change in the coal seams. The coal deformability will decrease, but the strain energy storage will be improved.

If the strain energy accumulates to the limit state and suddenly releases, the coal mass will be damaged by irreversible instability. If the strain energy release process is not effectively controlled, disasters and accidents may result due to mining disturbance or gas extraction.

To better understand the effects of pre-mining unloading expansion simulation (PUES) of PCM, coal sample P-2-1 as a control group sample did not undergo the pre-mining pressure relief and permeability enhancement simulation, while the other three specimens with gas pressures equal to 2 MPa underwent the simulations. The testing results are shown in Figures 9 and 10 and Table 4, which show that irreversible volume strain is produced during the PUES process; that is, the unloading damage is caused by pre-mining stress unloading and deformability changes. The mining-induced mechanical behavior of the coal mass in PCM with a gas pressure equal to 2 MPa is shown in the stress-strain curves in Figure 9, where the residual strain induced by the PUES is not counted. The axial strain induced by the unit axial stress increment and the amount corresponding to the peak stress of the coal samples with PUES are larger than that of coal samples without PUES. The volume strain of coal samples with PUES increases slowly before the peak stress and growth is accelerated after the peak stress, while the volume strains of the coal samples without PUES show the opposite evolution, i.e., the volume strain growth rate is faster than that of the coal samples with PUES, but the growth rate slows down in the post-peak section. The above test results show that the PUES promotes the axial deformation capacity and anisotropy of the coal deformability, and the deformability of the coal mass with PUES significantly increases in the post-peak section, which has a direct impact on the initial coal permeability change before the mining practice.

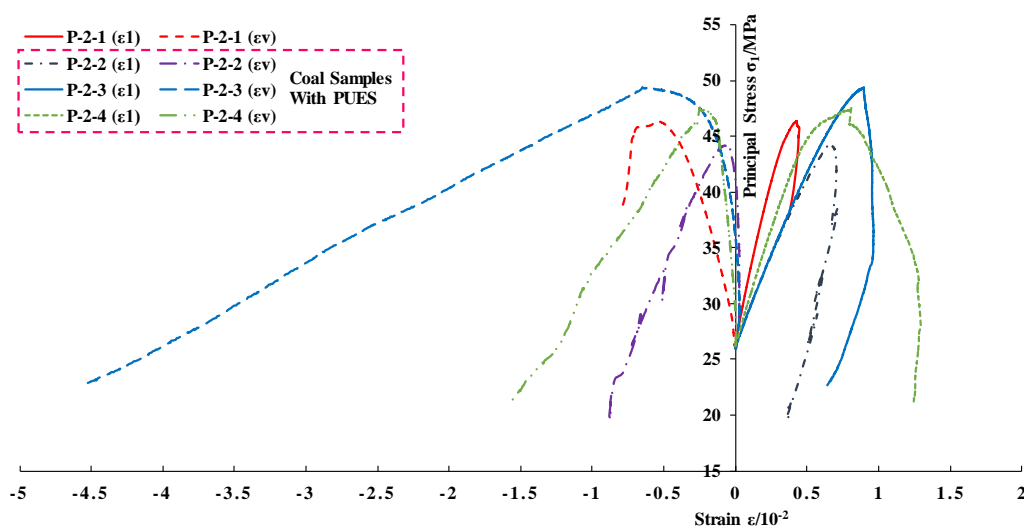


Figure 9. The mining-induced mechanical behavior of coal under PCM with a 2 MPa gas pressure difference.

According to Table 4 and Figure 10, the peak stress and corresponding confining pressure decrease in the order of NM, TCM and PCM under the same gas pressure, and all the calculated stress concentration coefficients (K), i.e., the ratio of peak stress to initial stress, are in the range of the coefficient measured in the corresponding mining layout. The peak stress of the coal samples under the same mining-induced stress conditions significantly decreases with the gas pressure.

According to Table 3 and Figure 10b,d, the absolute values of the axial strain and circumferential strain corresponding to the peak stress generally decrease and the volume strain increases in the order of NM, TCM and PCM under the same gas pressure. The volume strain is negative when the specimen is destroyed, i.e., volume expansion occurred when the specimen was destroyed. The volumetric strain corresponding to the peak stress obviously increases with increasing gas pressure under the same mining-induced stress conditions. The test results of the individual samples are slightly different from those of the whole test, which is related to the dispersion of the raw coal samples. The influence of mining-induced stress conditions on the mechanical behavior of coal is higher than the gas pressure influence.

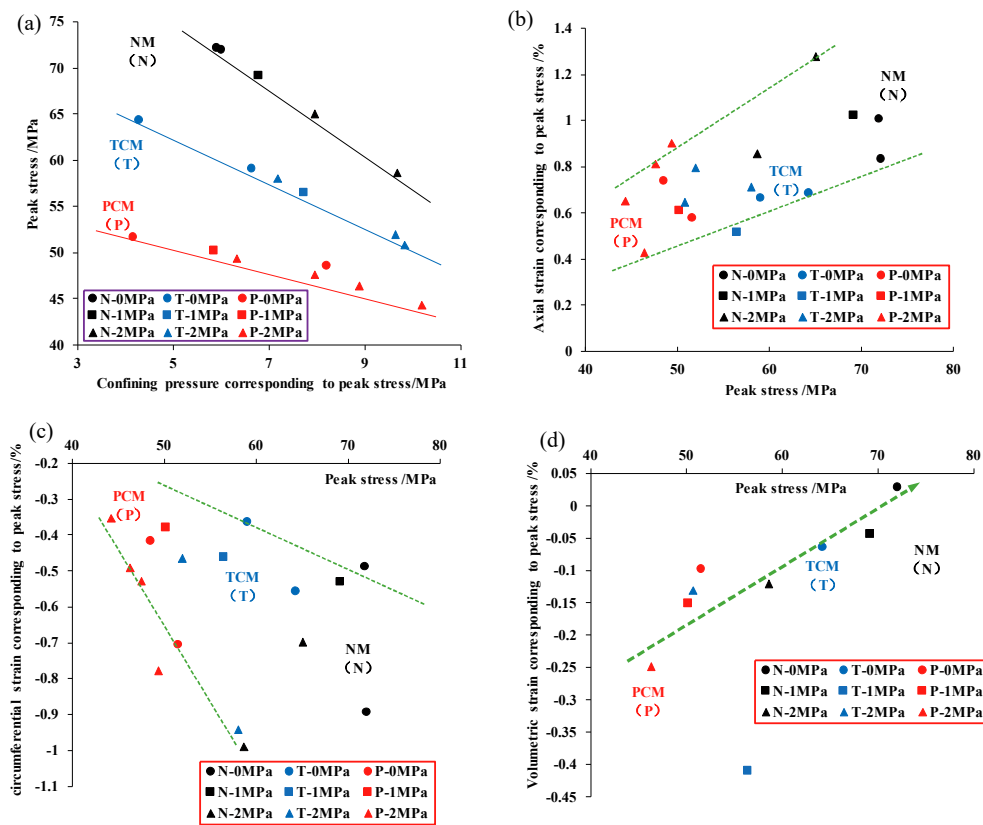


Figure 10. Peak stress and corresponding mechanical parameters under different mining-induced stress conditions: (a) peak stress and the corresponding confining pressure; (b) peak stress and the corresponding axial strain; (c) peak stress and the corresponding circumferential strain; (d) peak stress and the volumetric strain.

Table 4. The test results of coal under different mining-induced stress conditions.

Sample Number	Peak Stress σ_1 /MPa	α	Test Values Corresponding to the Peak Stress				Peak Permeability/mD	
			σ_3 /MPa	$\epsilon_1/10^{-2}$	$\epsilon_3/10^{-2}$	$\epsilon_v/10^{-2}$		
N-0-1	72.14	2.89	5.92	0.831	-0.895	-0.959	No gas flow conditions	
N-0-2	71.92	2.87	6.01	1.004	-0.488	0.028		
T-0-1	64.32	2.57	4.30	0.683	-0.558	-0.433		
T-0-2	59.06	2.36	6.65	0.665	-0.365	-0.065		
P-0-1	51.62	2.06	4.18	0.577	-0.707	-0.838		
P-0-3	48.60	1.94	8.21	0.739	-0.418	-0.098		
N-1-1	69.19	2.77	6.78	1.021	-0.532	-0.044	0.853	9.886
T-1-1	56.49	2.26	7.73	0.515	-0.462	-0.410	0.016	9.697
P-1-1	50.19	2.01	5.85	0.610	-0.380	-0.151	0.022	10.380
N-2-1	58.67	2.35	9.67	0.858	-0.989	-1.121	0.224	0.238
N-2-2	65.03	2.60	7.95	1.278	-0.699	-0.120	0.212	2.552
T-2-1	50.77	2.03	9.84	0.646	No data due to equipment failure			
T-2-2	58.04	2.32	7.18	0.713	-0.943	-1.173	0.209	0.445
T-2-3	52.00	2.08	9.64	0.797	-0.464	-0.131	0.534	2.466
P-2-1	46.35	1.85	8.88	0.429	-0.491	-0.553	0.299	0.462
P-2-2	44.28	1.77	10.20	0.652	-0.354	-0.056	0.380	1.675
P-2-3	49.40	1.98	6.33	0.901	-0.777	-0.653	0.307	2.311
P-2-4	47.59	1.90	7.96	0.811	-0.529	-0.248	0.244	2.548

The morphologies of the coal samples before and after loading are shown in Figure 11. The failure forms of the coal samples with no gas permeability under different mining-induced stress conditions are tensile-shear failure; the main shear section penetrates the specimen, and the crack opening near the shear surface is large. The fragmentation degree of the coal specimens decreases in accordance with the order of NM, TCM and PCM. The failure forms of the coal samples with gas permeability under different mining-induced stress conditions are mainly shear failure, and the shear surface becomes the main seepage channel. However, due to the particularity of the coal samples, the gas flow in the coal mass and corresponding permeability evolution are seriously influenced by the regional or specific damage to the coal mass, e.g., the end of coal sample T-2-1 is greatly damaged in the tests, and the deformation is too large, resulting in slipping of the circumferential extensometer during the test, and the circumferential deformation and seepage flow parameters of the coal were not recorded. However, the coal sample's final failure form is related to the initial fracture distributions, based on which the mining-induced fracture network generates and maintains an influence on the mechanical behavior and gas permeability in the coal mass under different mining-induced stress conditions and gas pressures.

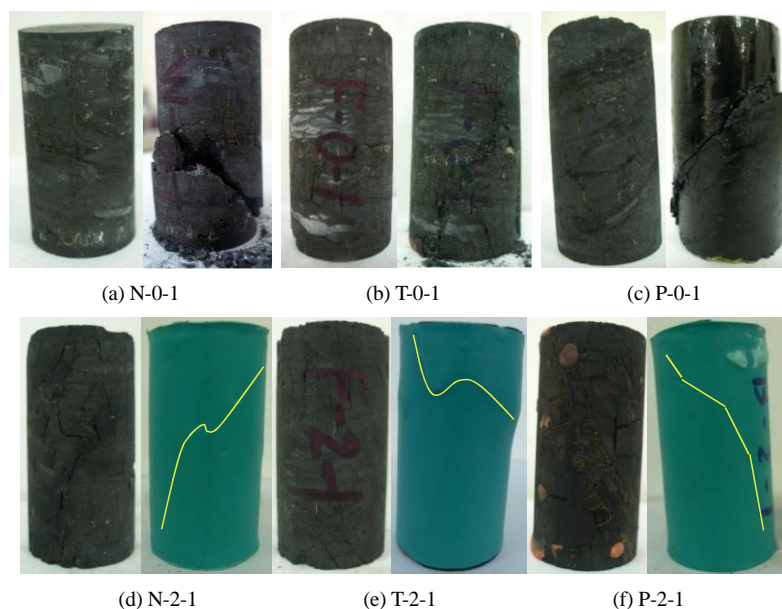


Figure 11. Images of coal samples before and after tests under different mining-induced stress conditions.

3.2.2. Gas Permeability Characteristics of Coal under Different Mining-Induced Stress Conditions

The relationships between the permeability and axial and circumferential strains in the coal mass under different mining-induced stress conditions are shown in Figure 12. The coal permeability evolution along with the deformation due to the mining-induced stress change can be divided into three sections, i.e., slowly increasing section, prepeak quickly increasing section and post-peak stable increasing section. In the slowly increasing section, the permeability of the coal samples at the beginning of loading and elastic deformation is basically constant or shows slow growth. In the pre-peak quickly increasing section, after entering the yield stress zone, the coal permeability begins to increase rapidly and continues to grow after the peak. In the post-peak stable increasing section, the coal permeability decreases due to the interruption of the existing connected seepage channel and then tends to stabilize.

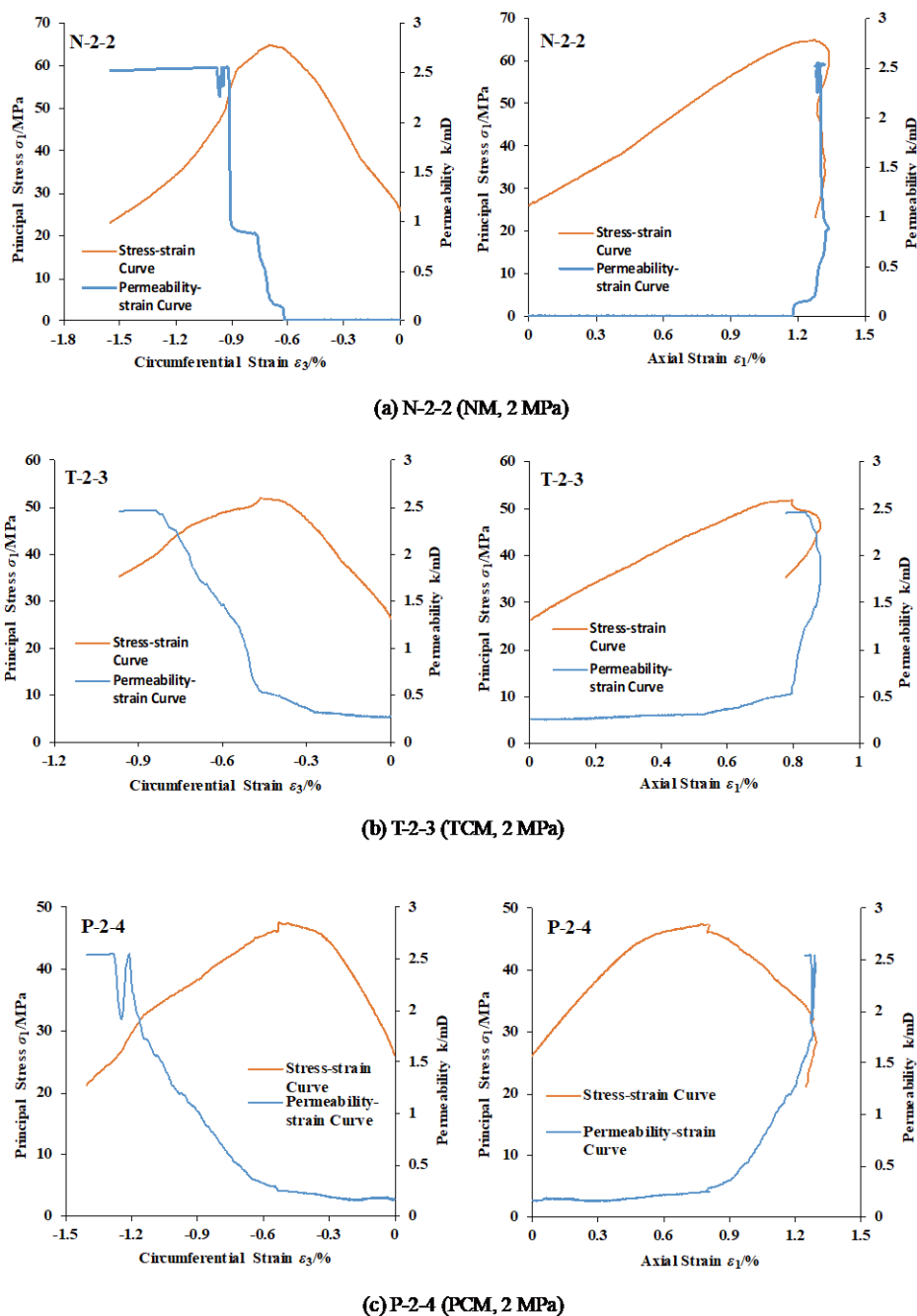


Figure 12. Permeability-strain curves of typical coal samples under different mining-induced stress conditions.

In contrast to the CTC test, the coal permeability does not decrease significantly at the initial stage of loading but greatly increases in the peak stress region in the mining-induced stress unloading experiments (MSUE). The coal permeability at the beginning of MSUE maintains constant or slow growth without an obvious decreasing section, which shows that under real mining-induced stress conditions, the coal permeability enhancement induced by stress unloading and coal permeability decrease caused by the axial compression are counteracted by each other; there is little change in the coal permeability before reaching the peak stress. Along with the stress loading, the coal rock mining-induced fracture expands and gradually connects based on the original natural fracture structures, forming macrofracture networks, and the coal permeability is greatly enhanced, which corresponds to the situation in which the broken coal near the mining face has high permeability.

4. Discussion

4.1. The Effects of Mining-Induced Stress Evolution on Volumetric Deformation and Permeability Enhancement of the Coal Mass

According to the comparison between the CTC and MSUE test results, the stress environment plays a controlling role in the mechanical behavior and permeability of coal, and the study of the mining-induced mechanical behavior and permeability of coal must consider the influence of the real mining-induced stress environment evolution process. To obtain a comprehensive understanding of the effects of mining-induced stress evolution on volumetric deformation and permeability enhancement of the coal mass, the stress-induced deformation must first be analyzed. Based on Hook's law, the volumetric strain of the coal mass can be calculated by the following relationship:

$$\varepsilon_v = \frac{1-2\mu}{E}(\sigma_1 + \sigma_2 + \sigma_3) = \frac{\sigma_m}{K} \quad (2)$$

where ε_v is the volumetric strain of the coal, μ is Poisson's ratio, E is the elastic modulus, σ is the principal stress, σ_m is the mean principal stress and K is the volumetric modulus of coal, which is equal to $3E/(1-2\mu)$.

With the advancement of mining, the stress state of a coal mass will change from an initially hydrostatic stress condition to a final uniaxial compression stress condition near the mining face, which is shown in Figure 13. The stress evolution will definitely influence the volumetric deformation process.

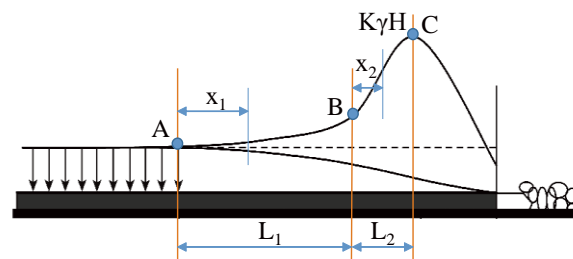


Figure 13. Abutment pressure distribution in front of the working face of the coal seam [36].

The stress evolution can be quantitatively described by the following equations [36]:

Section AB:

$$\begin{cases} S_1 = \frac{3x_1}{5L_1}\gamma H \\ \sigma_1 = \left[1 + \frac{x_1}{2L_1}\right]\gamma H \\ \sigma_3 = \left[1 - \frac{2x_1}{5L_1}\right]\gamma H \\ \sigma_m = \left[1 - \frac{x_1}{10L_1}\right]\gamma H \end{cases} \quad (3)$$

Section BC:

$$\begin{cases} S_1 = \left[0.6 + \frac{x_2}{L_2}(\alpha - 0.733)\right]\gamma H \\ \sigma_1 = \left[1.5 + \frac{x_2}{L_2}(\alpha - 1.5)\right]\gamma H \\ \sigma_3 = \left[0.6 - \frac{2x_2}{5L_2}\right]\gamma H \\ \sigma_m = \left[0.9 + \frac{(\alpha - 2.3)x_2}{3L_2}\right]\gamma H \end{cases} \quad (4)$$

where S is the deviatoric stress, α is the stress concentration factor, x represents the distance from a point in the section to the start of the section, L_1 and L_2 represent the lengths of the sections, H is the depth, and γ represents the overburden density (N/m^3).

Then, the volumetric strain can be calculated by the following equations:

Section AB:

$$\varepsilon_v = \left[1 - \frac{x_1}{10L_1}\right] \frac{\gamma H}{K} \quad (5)$$

Section BC:

$$\varepsilon_v = \left[0.9 + \frac{(\alpha - 2.3)x_2}{3L_2} \right] \frac{\gamma H}{K} \quad (6)$$

Based on Equations (5) and (6), the volume strain increases with the advancement of mining, i.e., the horizontal stress decreases and the vertical stress increases.

According to Zhang et al.'s research [22], the increment of the coal permeability Δk can be calculated as follows:

$$\Delta k = \left[\left(1 - \frac{\varepsilon_v}{\phi_0} \right)^{\alpha_\phi} / (1 - \varepsilon_v)^{\alpha_\phi} - 1 \right] \times k_0 \quad (7)$$

where α_ϕ is the porosity sensitivity exponent, which is typically greater than two for coal, ϕ is the porosity of coal and subscript 0 indicates the initial value. According to Equation (7), the coal permeability increases with the volume expansion, which is mainly induced by the advancement of mining and corresponding change in the stress environment, as shown in Equations (5) and (6).

As shown in Figure 10d, significant volume expansions in the coal samples were caused by the indoor test simulation, which was designed according to the actual mining-induced stress environment evolution process, which also made the coal sample permeability evolution process different from the CTC test results, and the permeability continued to increase without decreasing section. The consistency of laboratory experimental results and the above-stated theoretical analyses also confirm the plausibility and practicality of MSU tests to truly reproduce the deformation and seepage law of in situ coal during the evolution of stress conditions in deep mining.

In addition, in the protection layer mining method simulation, the PUES of the coal mass in the protected coal seams is conducted, resulting in the residual volume expansion strain of the coal samples, which results in obvious pre-mining permeability enhancement of the coal samples. This result fully demonstrates that the PCM can greatly improve the permeability of the protected coal seams. If cross layer gas extraction and other engineering technologies can reasonably cooperate, the risk of coal and gas outbursts can be significantly reduced during the mining process of the protected coal seam.

Because of the generally ultralow permeability of coal seams in China, it is impossible to directly introduce direct CBM extraction technology from the United States and other countries. Faced with the demand for a large number of high gas content and low permeability coal seams in China, the first problem to be solved is how to improve the permeability of the coal seam in the extraction area and promote gas desorption in the coal seams, which can improve the extraction efficiency. According to the present theoretical and experimental results, the most effective means of coal permeability enhancement is pressure relief, and the primary objective of engineering measures is to increase the volume strain of the coal mass. The extraction time and key extraction region should be optimized using the theory of mining-induced coal permeability enhancement.

4.2. The Effects of Gas Pressure on Coal Permeability under MSU Conditions

The coal permeability and mechanical behavior are deeply influenced by the stress conditions [43]. In coal mining and CBM extraction practices, the mining-induced volumetric strain will lead to obvious gas pressure evolution [44], which deeply influences the gas sorption/desorption processes, permeability [45] and effective stress changes in the coal mass [46].

Based on the isotherm gas sorption theory, the gas adsorption is linearly related to gas pressure. The sorption-induced volumetric free swelling strain change $\Delta\varepsilon_s$ in the coal blocks can be calculated by the following relationship [23]:

$$\Delta\varepsilon_s = \frac{\varepsilon_L p}{p + p_L} - \frac{\varepsilon_L p_0}{p_0 + p_L} \quad (8)$$

where p is the gas pressure, p_0 is the initial gas pressure, ε_L is the maximum volumetric swelling strain and p_L is the Langmuir pressure constant. Based on Equation (8), volumetric expansion in the coal mass increases with increasing gas pressure. However, as the gas pressure decreases, there will be shrinkage deformation in the coal mass. Considering that the compressibility of the coal matrix is

much smaller than that of the coal pores and fractures, the volumetric strain evolution induced by gas pressure change mainly occurs in the open pores and fractures in coal, resulting in a further influence on the coal permeability and macromechanical response.

Many rock mechanics studies also show that as long as there are connected pore systems in rocks, the Terzaghi effective stress law [47], which has been proven in soil mechanics, can also be applied in rocks. However, for coal and some other rocks with a high degree of cementation and unconnected pore systems, the Terzaghi effective stress law is not adequately accurate. Corresponding studies have shown that the gas pressure is an important parameter of the effective stress in gas-containing coal. The effective stress in the coal mass can be expressed as follows [48]:

$$\begin{cases} \sigma_e = \sigma - \beta p \\ \beta = \frac{2\varepsilon_L \rho RT(1-2\mu) \ln(1+p_L p)}{3Vp} \end{cases} \quad (9)$$

where β is the equivalent pore pressure coefficient, ρ is the apparent density of coal, R is a general gas constant and equals 8.3143 J/(mol·K), T is absolute temperature (K), μ is Poisson's ratio of coal, and V is the volume of a mole of gas at standard atmospheric pressure and equals $22.4 \times 10^{-3} \text{ m}^3/\text{mol}$.

Based on Equation (9), the equivalent pore pressure coefficient β is a variable and decreases with increasing gas pressure. Then, the effective stress increment can be obtained by the following relationship:

$$\Delta\sigma_e = \Delta\sigma - 2\varepsilon_L \rho RT(1-2\mu) \ln(1+p_L \Delta p) \quad (10)$$

According to Equation (10), the effective stress variation is introduced by the evolution of total stress and adsorptive gas pressure. The effective stress increases with the decrease in gas pressure, which has been proven by many studies and results in a coal matrix compression deformation [36].

Based on the abovementioned analyses, the gas pressure also affects the seepage mechanical properties of coal by controlling the gas sorption/desorption process and the effective stress evolution. As an adsorptive gas, the CBM can introduce adsorption expansion strain or desorption shrinkage strain in a coal mass according to the increase or decrease in gas pressure, resulting in a change in the amount and spatial distribution of the effective seepage channels in the coal mass. Typically, the sorption-induced strain and effective stress in a coal mass and coal permeability have the following relationship [23]:

$$k = k_0 \left[\exp(-C_f \Delta\sigma_e) - \frac{f}{\phi_{f0}} \times \Delta\varepsilon_s \right]^3 \quad (11)$$

where C_f is the compressibility of coal fractures, f is the partition factor of gas sorption-induced swelling strain contributing to the fracture aperture change, ϕ_{f0} is the initial fracture porosity of the coal, and σ_e is the effective stress.

Substituting Equations (8) and (10) into Equation (11), the relationship between the coal permeability and gas pressure can be further derived as follows:

$$k = k_0 \left[\exp\{-C_f [\Delta\sigma - 2\varepsilon_L \rho RT(1-2\mu) \ln(1+p_L \Delta p)]\} - \frac{f}{\phi_{f0}} \times \left(\frac{\varepsilon_L p}{p+p_L} - \frac{\varepsilon_L p_0}{p_0+p_L} \right) \right]^3 \quad (12)$$

According to Equation (12), the coal permeability increases with the increment of gas desorption-induced shrinkage strain resulting from the decrease in gas pressure. Therefore, the coal permeability could be enhanced by reducing the gas pressure if the total stress variation is neglected, which has also been laterally verified by our test results. In Table 4, the peak permeabilities of the coal samples with gas flow pressure differences equal to 1 MPa are obviously larger than those of coal samples with 2 MPa gas pressure differences.

However, mining practices can introduce significant stress unloading, while the gas pressure also correspondingly changes with mining-induced coal permeability enhancement and CBM extraction-induced gas desorption and migration. MSU is a complex process, which can introduce

significant volumetric expansion in a coal mass, resulting in an obvious effective stress unloading and coal permeability enhancement. CBM extraction is usually conducted simultaneously during the process of gas-rich coal seam mining, especially in mining-induced pressure relief and permeability enhancement sections. The gas pressure in the coal seams continuously decreases due to the CBM extraction and mining-induced coal permeability enhancement, and the gas adsorbed in the coal pores desorbs into the gas flow channel during the process of CBM extraction. The gas pressure reduction also causes decreases in effective stress and permeability in coal seams and results in compression deformation competing with mining-induced expansion deformation in the coal mass. This competition is particularly prominent in the mining process of high gas pressure coal seams, which are typically located in deep underground and key areas of future mining practices.

Therefore, to guarantee the safe and efficient development of simultaneous deep coal and gas extraction practices, the quantity control of CBM extraction and gas pressure should be coordinated with the mining-induced stress spatiotemporal evolution, i.e., for high gas pressure coal seams, it is not urgent to reduce gas pressure in the coal seams, and for low gas pressure coal seams, advancing pressure relief should be conducted to improve coal seam permeability and CBM extraction efficiency.

4.3. The Failure Mechanism of a Coal Mass Considering MSU and Gas Pressure Effects

Based on the Mohr-Coulomb strength criterion, a rock mass fails when the ratio of shear stress to normal stress on the shear plane reaches the maximum. The mathematical expression of the Mohr-Coulomb strength envelope is as follows:

$$\tau = \sigma \tan \varphi + c \quad (13)$$

where τ is the shearing strength, φ is the internal friction angle, and c is the cohesion.

Considering the effects of pore pressure and mining-induced deterioration of the strength parameters, the strength envelope can be stated as follows:

$$\tau_u = (\sigma - \beta p) \tan \varphi_u + c_u \quad (14)$$

where subscript u represents the stress unloading conditions, and the internal friction angle and cohesion of the coal mass under specific stress unloading conditions can be calculated with the following formulas [49]:

$$\begin{cases} \varphi_u = \arcsin \left[\frac{(\sigma'_1 - \sigma'_3) - (\sigma_1 - \sigma_3)}{(\sigma'_1 + \sigma'_3) - (\sigma_1 + \sigma_3)} \right] \\ c_u = \frac{(\sigma_1 - \sigma_3) - (\sigma_1 + \sigma_3) \sin \varphi_u}{2 \cos \varphi_u} \end{cases} \quad (15)$$

where $\sigma'_1, \sigma'_3, \sigma_1$ and σ_3 are the principal stresses at different stress states. The mechanical parameters of unloading the rock mass can decline by up to half of the initial value [49].

According to the abovementioned analyses, the existence of gas pressure reduces the effective stress in the coal mass; therefore, the minimum effective stress is less than the minimum principal stress. Then, if we conduct CTC tests, the minimum effective stress is the actual confining pressure and remains constant, while the maximum effective stress continues to increase until the Mohr circle is tangent to the strength envelope of the CTC tests and the rock sample is damaged (Figure 14). However, the mechanical parameters obtained by the CTC tests represent only the intrinsic mechanical properties of materials, and the mechanical behavior cannot represent the actual mechanical response of a mining-influenced coal mass. To simulate mining-induced stress unloading conditions, MSU tests with gas flow conditions should be conducted. The minimum effective stress is the confining pressure and continues to decrease, while the maximum effective stress continues to increase until the Mohr circle is tangent to the strength envelope of the MSU tests and the rock sample is damaged (Figure 14).

For a specific rock material, the strength envelopes are fixed. The failure strength of the coal mass under real mining-induced stress evolution conditions, i.e., in the MSU tests, is much lower

than that of the CTC tests. If the gas pressure is increasing, the failure strength of the coal mass is even smaller due to the limit of the strength envelope. By controlling the weakened mechanical parameter of the coal mass, the mining-induced stress evolution and actual gas pressure conditions play a decisive role in the damage failure of mining-influenced coal mass. It is necessary to focus on the mining-influenced mechanical parameters of a coal mass in the process of conducted deep gas-rich coal seam mining practices.

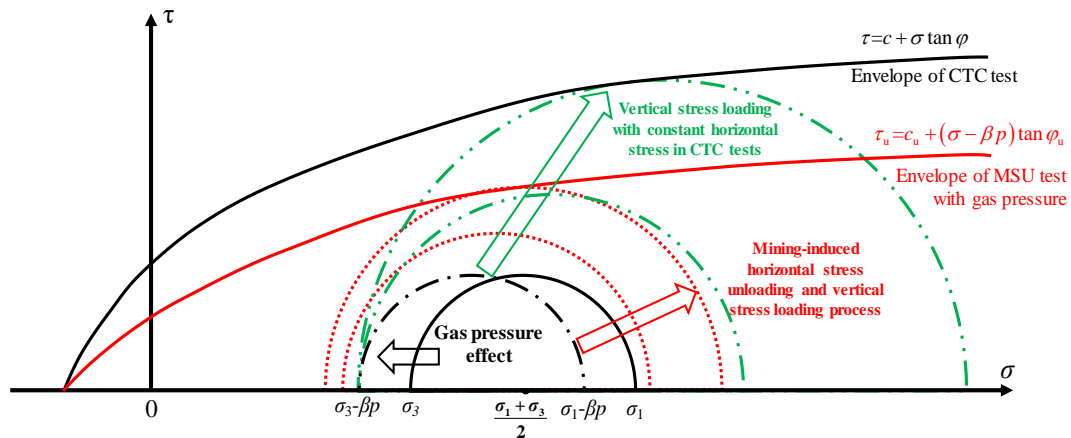


Figure 14. The mechanism of mining-induced stress unloading and gas pressure on coal strength.

5. Conclusions

Mining-induced stress conditions and gas pressures always affect the mechanical behavior and permeability evolution of the coal mass, which is also the major concern in deep coal mining and CBM extractions. To obtain the real mining-induced coal mechanical response and coal permeability characteristics, a series of stress unloading experiments with different gas pressures to simulate the mining-induced stress evolution processes induced by three typical mining layouts were conducted. The testing results are also compared with those of the CTC tests conducted under different gas pressures, and the different mechanisms between the methods are theoretically analyzed.

The mining-induced stress evolution and gas pressure change do have an impact on the gas permeability and mechanical response of coal. The testing results show that the strength, axial strain and circumferential strain corresponding to the peak stress of a coal mass under different mining layouts decrease in the order of NM, TCM and PCM, while the absolute value of the volumetric strain increases in that order under the same gas pressure. Under the same mining-induced stress conditions, the strength of the coal mass decreases with increasing gas pressure, while the absolute deformation of the coal mass increases. Under real mining-induced stress conditions, the volumetric strain of the coal mass remains negative, indicating that the volume of the coal mass continues to increase. The volumetric strain corresponding to the peak stress of the coal mass increases with gas pressure under the same mining-induced stress conditions. In the CTC tests, the coal mass volume continues to decrease and always in a compression state, and there is not an obvious deformation platform that appears in the MSU tests.

The deformation and seepage capacity evolution processes of coal under different mining layouts can be divided into three sections: slow increase, fast increase and decrease-stable. The coal permeability variation range in the MSU test is much higher than that in the CTC tests. The coal permeability typically decreases initially and begins to increase after reaching the yield deformation stage in the CTC tests. However, in the MSU simulation test, the permeability of the coal mass continuously increases before reaching the peak stress and decreases in the postpeak section. The effective stress evolution with the generation of coal fracture networks plays a key role in determining the gas permeability and mechanical behavior of mining-induced coal mass.

Both theoretical and experimental analyses show that MSU and gas pressure changes greatly impact deformation and permeability enhancement of a coal mass, and the failure mechanism is also seriously influenced by MSU and gas pressure change-induced effective stress variations. The mechanical parameters of the coal mass are influenced by the process of deep gas-rich coal seam mining practices.

Author Contributions: Conceptualization, Z.Z. and R.Z.; Data curation, Y.Z.; Formal analysis, Z.C.; Funding acquisition, Z.Z., R.Z. and Z.C.; Investigation, M.G. and Y.Z.; Methodology, Z.Z.; Project administration, R.Z.; Supervision, R.Z. and M.G.; Validation, M.G. and J.X.; Visualization, J.X.; Writing—original draft, Z.Z.; Writing—review & editing, R.Z. All authors have read and agreed to the published version of the manuscript.

Funding: This research was funded by the National Natural Science Foundation of China (No. U1965203, 51804204), the Open Fund of State Key Laboratory of Water Resource Protection and Utilization in Coal Mining (Grant No. SHJT-17-42.13), the China Postdoctoral Science Foundation (2019T120841), the Applied Basic Research Programs of Sichuan Province (No. 2019YJ0136), the SCU Full-time Postdoctoral Research and Development Foundation (2017SCU12025), the Open Foundation of MOE Key Laboratory of Deep Underground Science and Engineering (DUSE201805).

Acknowledgments: We would like to deliver our great thanks to Zhaopeng Zhang and Yang Liu from MOE Key Laboratory of Deep Earth Science and Engineering (Sichuan University) for the help in conducting the experimental tests. Reprinted by permission from Springer Rock Mechanics and Rock Engineering. Zhang Z., et al. Mining—induced coal permeability change under different mining layouts, 2016, 49(9):3753–3768.

Conflicts of Interest: The authors declare no conflict of interest.

Nomenclature

Latin Symbols

A	Cross section of the specimen, m^2 ;
c	Cohesion, MPa;
C_f	Compressibility of coal fractures, MPa^{-1} ;
E	Elastic modulus, GPa;
f	Partition factor of gas sorption-induced swelling strain contributing to the fracture aperture change, %;
H	Depth, m;
k	Permeability, mD;
K	Volumetric modulus of coal, GPa;
L	Length of the coal specimen, m;
p	Gas pressure, MPa;
p_L	Langmuir pressure constant, MPa;
q	Flow rate, m^3/s ;
R	General gas constant, J/(mol·K);
S	Deviatoric stress, MPa;
T	Absolute temperature, K;
V	Volume of a mole of gas at standard atmospheric pressure, $22.4 \times 10^{-3} m^3/mol$;

Greek Symbols

α	Stress concentration factor, dimensionless;
α_ϕ	Porosity sensitivity exponent, dimensionless;
β	Equivalent pore pressure coefficient, dimensionless;
γ	Overburden density, N/m^3 ;
ε	Strain, %;
ε_L	Maximum volumetric swelling strain, %;
Δ	Increment, dimensionless;
μ	Poisson's ratio, dimensionless;
μ_v	Viscosity coefficient of gas, Pa·s;
ρ	Apparent density of coal, N/m^3 ;
σ	Stress, MPa;
τ	Shearing strength, MPa;
ϕ	Porosity, %;
φ	Friction angle, °;

Abbreviations

CBM	Coalbed methane;
CT	Computed tomography
CTC	Conventional triaxial compression
ECBM	Enhanced coalbed methane
MSU	Mining-induced stress unloading
NM	Non-pillar mining
PCM	Protective coal-seam mining
PUES	Premining unloading-expansion simulation
TCM	Top-coal caving mining

Superscripts and Subscripts

0	Initial value;
e	Effective stress;
f	Fracture;
L	Langmuir;
s	Sorption;
u	Stress unloading conditions;

References

1. IPCC. Summary for Policymakers. In *Global Warming of 1.5 °C. An IPCC Special Report on the Impacts of Global Warming of 1.5 °C Above Pre-Industrial Levels and Related Global Greenhouse Gas Emission Pathways, in the Context of Strengthening the Global Response to the Threat of Climate Change, Sustainable Development, and Efforts to Eradicate Poverty*; IPCC: Geneva, Switzerland, 2018; pp. 1–33.
2. Seneviratne, S.I.; Rogelj, J.; Seferian, R.; Wartenburger, R.; Allen, M.; Cain, M.; Millar, R.J.; Ebi, K.L.; Ellis, N.; Hoegh-Guldberg, O.; et al. The many possible climates from the Paris Agreement's aim of 1.5 °C warming. *Nature* **2018**, *558*, 41–49. [[CrossRef](#)] [[PubMed](#)]
3. Yan, H.; Zhang, J.; Zhao, Y.; Zheng, C. CO₂ Sequestration from flue gas by direct aqueous mineral carbonation of wollastonite. *Sci. China Ser. E Technol. Sci.* **2013**, *56*, 2219–2227. [[CrossRef](#)]
4. Young, A.L. Coalbed Methane: A New Source of Energy and Environmental Challenges. *Environ. Sci. Pollut. Res.* **2005**, *12*, 318–321. [[CrossRef](#)] [[PubMed](#)]
5. Montzka, S.A.; Dlugokencky, E.J.; Butler, J.H. Non-CO₂ greenhouse gases and climate change. *Nature* **2011**, *476*, 43–50. [[CrossRef](#)] [[PubMed](#)]
6. Tutak, M.; Brodny, J. Forecasting Methane Emissions from Hard Coal Mines Including the Methane Drainage Process. *Energies* **2019**, *12*, 3840. [[CrossRef](#)]
7. Solomon, S.; Qin, D.; Manning, M.; Chen, Z.; Marquis, M.; Averyt, K.B.; Tignor, M.; Miller, H.L. (Eds.) *Climate Change 2007: The Physical Science Basis. Contribution of Working Group I to the Fourth Assessment Report of the Intergovernmental Panel on Climate Change*; Cambridge University Press: Cambridge, UK, 2007.
8. Jarosław, B.; Magdalena, T. The Use of Artificial Neural Networks to Analyze Greenhouse Gas and Air Pollutant Emissions from the Mining and Quarrying Sector in the European Union. *Energies* **2020**, *13*, 1–31.
9. Zhou, F.; Hou, W.; Allinson, G.; Wu, J.; Wang, J.; Cinar, Y. A feasibility study of ECBM recovery and CO₂ storage for a producing CBM field in Southeast Qinshui Basin, China. *Int. J. Greenh. Gas Control.* **2013**, *19*, 26–40. [[CrossRef](#)]
10. Busch, A.; Gensterblum, Y. CBM and CO₂-ECBM related sorption processes in coal: A review. *Int. J. Coal Geol.* **2011**, *87*, 49–71. [[CrossRef](#)]
11. Ujihira, M.; Higuchi, K.; Mizuma, H. On the Triaxial Compression Test of Coal and other Specimens in Which High Pressure Gas is Involved. *J. Geophys. Res.* **1985**, *106*, 21475–21494.
12. Bukowska, M. Mechanical Properties of Carboniferous Rocks in the Upper Silesian Coal Basin under Uniaxial and Triaxial Compression Tests. *J. Min. Sci.* **2005**, *41*, 129–133. [[CrossRef](#)]
13. Hobbs, D.W. The Strength and the Stress-Strain Characteristics of Coal in Triaxial Compression. *J. Geol.* **1964**, *72*, 214–231. [[CrossRef](#)]
14. Kong, X.; Wang, E.; Hu, S.; Shen, R.; Li, X.; Zhan, T. Fractal characteristics and acoustic emission of coal containing methane in triaxial compression failure. *J. Appl. Geophys.* **2016**, *124*, 139–147. [[CrossRef](#)]

15. Xie, H.P.; Zhou, H.W.; Liu, J.F.; Gao, F.; Zhang, R.; Xue, D.J.; Zhang, Y. Mining-induced mechanical behavior in coal seams under different mining layouts. *J. China Coal Soc.* **2011**, *36*, 1067–1074.
16. Xie, H.; Gao, F.; Ju, Y. Research and development of rock mechanics in deep ground engineering. *Chin. J. Rock Mech. Eng.* **2015**, *34*, 2161–2178.
17. Diederichs, M.; Kaiser, P.; Eberhardt, E. Damage initiation and propagation in hard rock during tunnelling and the influence of near-face stress rotation. *Int. J. Rock Mech. Min. Sci.* **2004**, *41*, 785–812. [[CrossRef](#)]
18. McKee, C.; Bumb, A.; Koenig, R. Stress-Dependent Permeability and Porosity of Coal and Other Geologic Formations. *SPE Form. Evaluat.* **1988**, *3*, 81–91. [[CrossRef](#)]
19. Feng, R.; Harpalani, S.; Pandey, R. Laboratory measurement of stress-dependent coal permeability using pulse-decay technique and flow modeling with gas depletion. *Fuel* **2016**, *177*, 76–86. [[CrossRef](#)]
20. Burgoyne, M.; Shrivastava, R. A practical workflow for characterizing stress-dependent behaviour of coal from changes in well productivity. *J. Nat. Gas Sci. Eng.* **2016**, *33*, 1025–1045. [[CrossRef](#)]
21. Xie, H.P.; Zhang, Z.T.; Feng, G.; Ru, Z.; Gao, M.Z.; Liu, J.F.; University, S. Stress-fracture-seepage field behavior of coal under different mining layouts. *J. China Coal Soc.* **2016**, *41*, 2405–2417.
22. Zhang, Z.; Zhang, R.; Xie, H.; Gao, M.; Xie, J. Mining-Induced Coal Permeability Change Under Different Mining Layouts. *Rock Mech. Rock Eng.* **2016**, *49*, 3753–3768. [[CrossRef](#)]
23. Chen, Z.; Liu, J.; Pan, Z.; Connell, L.D.; Elsworth, D. Influence of the effective stress coefficient and sorption-induced strain on the evolution of coal permeability: Model development and analysis. *Int. J. Greenh. Gas Control* **2012**, *8*, 101–110. [[CrossRef](#)]
24. Palmer, I.; Mansoori, J. How Permeability Depends on Stress and Pore Pressure in Coalbeds: A New Model. *SPE Reserv. Evaluat. Eng.* **1998**, *1*, 539–544. [[CrossRef](#)]
25. Shi, J.-Q.; Durucan, S. Drawdown Induced Changes in Permeability of Coalbeds: A New Interpretation of the Reservoir Response to Primary Recovery. *Transp. Porous Media* **2004**, *56*, 1–16. [[CrossRef](#)]
26. Cui, X.; Bustin, M. Volumetric strain associated with methane desorption and its impact on coalbed gas production from deep coal seams. *AAPG Bull.* **2005**, *89*, 1181–1202. [[CrossRef](#)]
27. Ju, Y.; Zhang, Q.; Zheng, J.; Wang, J.; Chang, C.; Gao, F. Experimental study on CH₄ permeability and its dependence on interior fracture networks of fractured coal under different excavation stress paths. *Fuel* **2017**, *202*, 483–493. [[CrossRef](#)]
28. Islam, R.; Hayashi, D.; Kamruzzaman, A. Finite element modeling of stress distributions and problems for multi-slice longwall mining in Bangladesh, with special reference to the Barapukuria coal mine. *Int. J. Coal Geol.* **2009**, *78*, 91–109. [[CrossRef](#)]
29. Zhang, M.; Shimada, H.; Sasaoka, T.; Matsui, K.; Dou, L. Evolution and effect of the stress concentration and rock failure in the deep multi-seam coal mining. *Environ. Earth Sci.* **2013**, *72*, 629–643. [[CrossRef](#)]
30. Wold, M.; Connell, L.D.; Choi, S. The role of spatial variability in coal seam parameters on gas outburst behaviour during coal mining. *Int. J. Coal Geol.* **2008**, *75*, 1–14. [[CrossRef](#)]
31. Singh, A.; Singh, R.; Maiti, J.; Kumar, R.; Mandal, P. Assessment of mining induced stress development over coal pillars during depillaring. *Int. J. Rock Mech. Min. Sci.* **2011**, *48*, 805–818. [[CrossRef](#)]
32. Zhang, Q.; Fan, X.; Liang, Y.; Li, M.; Li, G.; Ma, T.; Nie, W. Mechanical Behavior and Permeability Evolution of Reconstituted Coal Samples under Various Unloading Confining Pressures—Implications for Wellbore Stability Analysis. *Energies* **2017**, *10*, 292. [[CrossRef](#)]
33. Zhang, R.; Ai, T.; Li, H.; Zhang, Z.; Liu, J. 3D reconstruction method and connectivity rules of fracture networks generated under different mining layouts. *Int. J. Min. Sci. Technol.* **2013**, *23*, 863–871. [[CrossRef](#)]
34. Xue, D.J.; Zhou, H.W.; Tang, X.L.; Zhao, Y.F. Mechanism of deformation-induced damage and gas permeability enhancement of coal under typical mining layouts. *Chin. J. Geotech. Eng.* **2013**, *35*, 328–336.
35. Xue, Y.; Dang, F.; Cao, Z.; Du, F.; Ren, J.; Chang, X.; Gao, F. Deformation, Permeability and Acoustic Emission Characteristics of Coal Masses under Mining-Induced Stress Paths. *Energies* **2018**, *11*, 2233. [[CrossRef](#)]
36. Zhang, Z.; Zhang, R.; Xie, H.; Gao, M.; Zha, E.; Jia, Z. An anisotropic coal permeability model that considers mining-induced stress evolution, microfracture propagation and gas sorption-desorption effects. *J. Nat. Gas Sci. Eng.* **2017**, *46*, 664–679. [[CrossRef](#)]
37. ASTM. *Standard Practices for Preparing Rock Core as Cylindrical Test Specimens and Verifying Conformance to Dimensional and Shape Tolerances*; American Society for Testing and Materials: West Conshohocken, PA, USA, 2008; Volume D4543.

38. Zhang, Z.; Ru, Z.; Liu, J.-F.; Liu, X.-H.; Li, J.-W. Permeability evolution of unloaded coal samples at different loading rates. *Therm. Sci.* **2014**, *18*, 1497–1504. [[CrossRef](#)]
39. Xie, H.; Zhao, X.; Liu, J.; Zhang, R.; Xue, D. Influence of different mining layouts on the mechanical properties of coal. *Int. J. Min. Sci. Technol.* **2012**, *22*, 749–755. [[CrossRef](#)]
40. Wang, S.; Elsworth, D.; Liu, J. Permeability evolution during progressive deformation of intact coal and implications for instability in underground coal seams. *Int. J. Rock Mech. Min. Sci.* **2013**, *58*, 34–45. [[CrossRef](#)]
41. Zhang, Z.; Zhang, R.; Li, G.; Li, H.; Liu, J. The Effect of Bedding Structure on Mechanical Property of Coal. *Adv. Mater. Sci. Eng.* **2014**, *2014*, 1–7. [[CrossRef](#)]
42. Biot, M.A. General Theory of Three-Dimensional Consolidation. *J. Appl. Phys.* **1941**, *12*, 155. [[CrossRef](#)]
43. Somerton, W.; Söylemezoglu, I.; Dudley, R. Effect of stress on permeability of coal. *Int. J. Rock Mech. Min. Sci. Géoméch. Abstr.* **1975**, *12*, 129–145. [[CrossRef](#)]
44. Xie, G.X.; Hu, Z.X.; Wang, L. Coal mining dilatancy characteristics of high gas working face in the deep mine. *J. China Coal Soc.* **2014**, *39*, 91–96.
45. Harpalani, S.; Chen, G. Influence of gas production induced volumetric strain on permeability of coal. *Geotech. Geol. Eng.* **1997**, *15*, 303–325. [[CrossRef](#)]
46. George, J.S.; Barakat, M. The change in effective stress associated with shrinkage from gas desorption in coal. *Int. J. Coal Geol.* **2001**, *45*, 105–113. [[CrossRef](#)]
47. Terzaghi, K. *Theoretical Soil Mechanics*; Wiley: New York, NY, USA, 1943.
48. Shi-Yue, W.U.; Wen, Z. Analysis of effective stress in adsorbed methane-coal system. *Chin. J. Rock Mech. Eng.* **2005**, *24*, 1674–1678.
49. Tao, L.; Zhou, K.; Jianhua, H.U.; Feng, G. Mechanics parameters deterioration laws of unloading rock mass by meso-damage mechanics. *J. Central South Univ.* **2013**, *44*, 275–281.



© 2020 by the authors. Licensee MDPI, Basel, Switzerland. This article is an open access article distributed under the terms and conditions of the Creative Commons Attribution (CC BY) license (<http://creativecommons.org/licenses/by/4.0/>).